Quantitative Evaluation of the Topographical Maps of Three-Dimensional Choroidal Vascularity Index in Children With Different Degrees of Myopia

Fang Liu,[1–3] Yuhao Ye,[1–3] Weiming Yang,[1–4] Jing Wang,[1–3] Ye Xu,[1–3] Yu Zhao,[1–3] Meng Li,[1–3] Zhi Chen,[1–3] Yang Shen,[1–3] Meiyan Li,[1–3] and Xingtao Zhou[1–3]

[1]Department of Ophthalmology and Optometry, Eye, Ear, Nose, and Throat Hospital, Fudan University, Shanghai, China
[2]NHC Key Laboratory of Myopia (Fudan University), Key Laboratory of Myopia, Chinese Academy of Medical Sciences, Shanghai, China
[3]Shanghai Research Center of Ophthalmology and Optometry, Shanghai, China
[4]Department of Ophthalmology, Children's Hospital of Fudan University, National Children's Medical Center, Shanghai, China

Correspondence: Xingtao Zhou, Department of Ophthalmology and Optometry, Eye, Ear, Nose, and Throat Hospital, Fudan University, No. 83 Fenyang Road, Shanghai 200031, China; doctzhouxingtao@163.com.
Meiyan Li, Department of Ophthalmology and Optometry, Eye, Ear, Nose, and Throat Hospital, Fudan University, No. 83 Fenyang Road, Shanghai 200031, China; limeiyan0406073@126.com.

Fang Liu and Yuhao Ye are joint first authors.
Xingtao Zhou and Meiyan Li contributed equally to the work presented here and should therefore be regarded as equivalent authors.

Received: July 4, 2023
Accepted: January 26, 2024
Published: March 11, 2024

Citation: Liu F, Ye Y, Yang W, et al. Quantitative evaluation of the topographical maps of three-dimensional choroidal vascularity index in children with different degrees of myopia. *Invest Ophthalmol Vis Sci.* 2024;65(3):14. https://doi.org/10.1167/iovs.65.3.14

Purpose. To investigate topographical maps of the three-dimensional choroidal vascularity index (3D-CVI) in children with different levels of myopia.

Methods. We enrolled 274 eyes from 143 children with various severity of myopia, including emmetropia (EM), low myopia (LM), and moderate–high myopia (MHM). The choroidal vessel volume (CVV), choroidal stroma volume (CSV), and 3D-CVI in different eccentricities (fovea, parafovea, and perifovea) and quadrants (nasal, temporal, superior, and inferior) were obtained from swept-source optical coherence tomography angiography (SS-OCTA) volume scans. All choroidal parameters were compared among groups, and the associated factors contributing to different 3D-CVIs were analyzed.

Results. Compared to the less myopic group, the more myopic group showed a significant decrease in CVV and CSV (MHM < LM < EM) and a significant increase in the 3D-CVI (MHM > LM > EM) in most areas (all $P < 0.05$). The nasal quadrant had the greatest 3D-CVI and lowest CSV and CVV, and vice versa in the temporal quadrant. The 3D-CVIs of the EM and LM groups gradually increased from the fovea to the perifovea, whereas the 3D-CVI of the MHM group first decreased and then increased. Regression analysis showed that axial length was an independent risk factor affecting foveal and parafoveal 3D-CVIs. Restricted cubic spline analysis revealed that the 3D-CVI increased with spherical equivalent (SE) when the SE was less than threshold and decreased when the SE was greater than threshold (SE thresholds for foveal, parafoveal, and perifoveal 3D-CVIs were −5.25 D, −5.125 D, and −2.00 D, respectively; all $P < 0.05$).

Conclusions. Children with myopia exhibited decreased CSV and CVV, increased 3D-CVIs, and altered 3D-CVI eccentricity characteristics (from the fovea to the perifovea). The quadratic relationship between the 3D-CVI and SE should be explored in longitudinal investigations.

Keywords: choroidal vascularity index, myopia, children

Myopia, a refractive error with a spherical equivalent (SE) of ≤−0.50 diopter (D), is the most common visual disorder worldwide and a major public health concern.[1] Early onset and rapid progression of myopia in children increase the risk of developing high or pathological myopia, which may result in a series of complications associated with visual impairment.[2,3] Numerous findings suggest that both genetic and environmental factors influence myopia progression.[4,5] Although the exact pathogenesis of myopia development remains unclear, the choroid has attracted growing interest due to its potential role in the onset and development of myopia.[6]

The choroid, located between the retinal pigment epithelium and sclera, is a highly vascularized tissue in the human body. It has been reported that the choroid adjusts the retinal position by changing its thickness in response to hyperopic or myopic optical defocus signals.[7,8] More recently, it has been proposed that the choroid regulates scleral extracellular matrix remodeling by releasing growth factors associated with oxygen and nutrient insufficiency.[9,10] Collectively, these reports suggest a critical role of the choroid in modulating eye growth and myopia progression.

However, there is a lack of reliable biomarkers to assess changes in the choroid due to its physical inaccessibility.

Recently, with rapid advances in optical coherence tomography (OCT) technology, there is increasing interest in a quantitative parameter known as the choroidal vascular index (CVI), which is the ratio of vascular area to total choroidal area. It has been reported that the CVI exhibits a lesser variability than choroidal thickness (ChT), as the coefficient of variation for the CVI has been reported to be 3.55 versus 40.30 for ChT.[11] Therefore, the three-dimensional choroidal vascularity index (3D-CVI) may be a more robust and reliable biomarker than the ChT to evaluate changes for choroid.[12–14] The CVI has been used to assess choroidal vascularity in various ocular diseases, including ametropia,[15] age-related macular degeneration,[13] and diabetic retinopathy.[14]

Given the regional variations of choroidal parameters in different eccentricities and quadrants,[16] choroidal parameters derived from volumetric scans rather than single-line scans will be less affected by local variations and therefore better represent the respective retinal zones. The CVI has been assessed with spatial considerations in normal populations,[17,18] but few reports have utilized volumetric scanning data. Recent studies have reported reduced choroidal vessel volume, stroma volume, and 3D-CVI in adult myopic eyes.[19,20] However, no such data have been reported in children with myopia. Therefore, this study is the first, to the best of our knowledge, to investigate topographical maps of the 3D-CVI and explore the influencing factors in children with various severity of myopia.

Materials and Methods

Patients

This observational, cross-sectional study was approved by the Ethics Review Board of the Eye, Ear, Nose, and Throat Hospital of Fudan University. Prior to the study, all participants and their parents received an explanation about the study, including the content, nature, and possible consequences of the study, and they provided written informed consent. All procedures were conducted in accordance with the tenets of the Declaration of Helsinki. Participants satisfying the following criteria were included: (1) age between 6 and 12 years, (2) best-corrected visual acuity (BCVA) $\geq$ 20/25, and (3) intraocular pressure (IOP) $<$ 21 mmHg. No participants had undergone orthokeratology or atropine myopia-control measures within the past 6 months. Participants with a history of systemic disease or intraocular surgery were excluded.

Ophthalmic Examination and Biometric Analysis

All participants underwent the following ophthalmic evaluations: BCVA, where the best-corrected vision with the use of glasses was measured with a standard logarithmic acuity chart at 5 m; IOP (Tonemeterx-10; Canon, Tokyo, Japan); white-to-white (WTW); central corneal thickness (CCT); mean corneal curvature (Km), the average between the K1 and K2 meridians; axial length (AL); anterior chamber depth; lens thickness (ZEISS IOLMaster 700; Carl Zeiss Meditec, Dublin, CA, USA); cycloplegic objective refraction (ARK-510A; NIDEK, Gamagori, Japan), with the examinations being performed 30 minutes after 0.5% tropicamide repeated three times at 5-minute intervals; and slit-lamp examination. Height, weight, and body mass index (BMI), calculated by dividing the height by the weight squared, were measured. Based on the SE of each eye, the participants were further divided into an emmetropia (EM) group, $\leq$+0.75 D and $>$−0.50 D; a low myopia (LM) group, $>$−3.0 D; and a moderate-to-high myopia (MHM) group, $\leq$−3.0 D.

Swept-Source OCT/OCT Angiography Image Analysis

After refractive errors measurement, swept-source OCT (SS-OCT) and SS-OCT angiography (SS-OCTA) examinations were performed by the same experienced ophthalmologist (FL) at a constant light level (30 lux) from 13:00 to 16:00 hours[21] to reduce the influence of daily rhythms and light exposure on the choroid.[22,23] SS-OCT/OCTA (VG200D; SVision Imaging, Ltd., Luoyang, China) images were captured using a swept-source laser with a wavelength of approximately 1050 nm and a speed of 200,000 A-scans per second. The maximum axial resolution, lateral resolution, and scanning depth were approximately 5 µm, 15 µm, and 3 mm, respectively. The volume data, including OCT and OCTA, were captured with a raster scan protocol of 512 A-scans × 512 B-scans repeated four times and averaged, covering a 9 × 9-mm area centered on the fovea with motion correction. The built-in algorithm was used to automatically segment the choroid, defined as the area from the outer edge of the retinal pigment epithelium–Bruch's membrane complex to the inner edge of the choroid–scleral interface. The deep learning (UNet) model was trained with 4476 B-scans and tested with 601 B-scans, and we obtained a 0.9327 Dice similarity coefficient (by comparing the model-predicted choroid boundary with those boundaries manually marked by experts at the pixel level), suggesting high reliability and repeatability. To further ensure segmentation accuracy, two trained doctors reassessed the choroidal boundary and manually segmented images that were inaccurately segmented, using built-in software.

Before quantitative analysis, AL values were imported into the system to adjust for magnified differences. The magnification formula (magnification of fundus *XY* measurement = 0.0492 × AL − 0.1818) was based on the optical design of the OCT system and the Navarro model.[24] All image analyses were performed using built-in software. The choroid vessel detection algorithm is based on the principle of adaptive threshold, the Niblack algorithm. The algorithm has been widely used to detect choroidal vessels.[25] It is further optimized using preprocessing and postprocessing steps to accommodate the range of vessel sizes and image contrasts typically observed in images, and it finally reconstructs the three-dimensional structure of the choroidal vasculature to obtain the map of choroidal vascularity (Fig. 1). This permits the automatic detection of Sattler's layer and Haller's layer without manual intervention. Accordingly, choroidal vessel volume (CVV) and the 3D-CVI (defined as the ratio of CVV to total choroidal volume, which reflects the volumetric vessel density of Sattler's layer and Haller's layer) were calculated automatically (Fig. 1). In this area, the larger the 3D-CVI, the larger the proportion of CVV. The macular zone was further divided into four different eccentricities (fovea, 0–1 mm; parafovea, 1–3 mm; perifovea, 3–6 mm; and near-periphery, 6–9 mm) according to Early Treatment Diabetic Retinopathy Study (ETDRS) grids (9 × 9-mm area). The choroidal stroma volume (CSV) was calculated as the total choroidal volume minus the CVV. Because the ALs of some participants were lower than

Investigative Ophthalmology & Visual Science

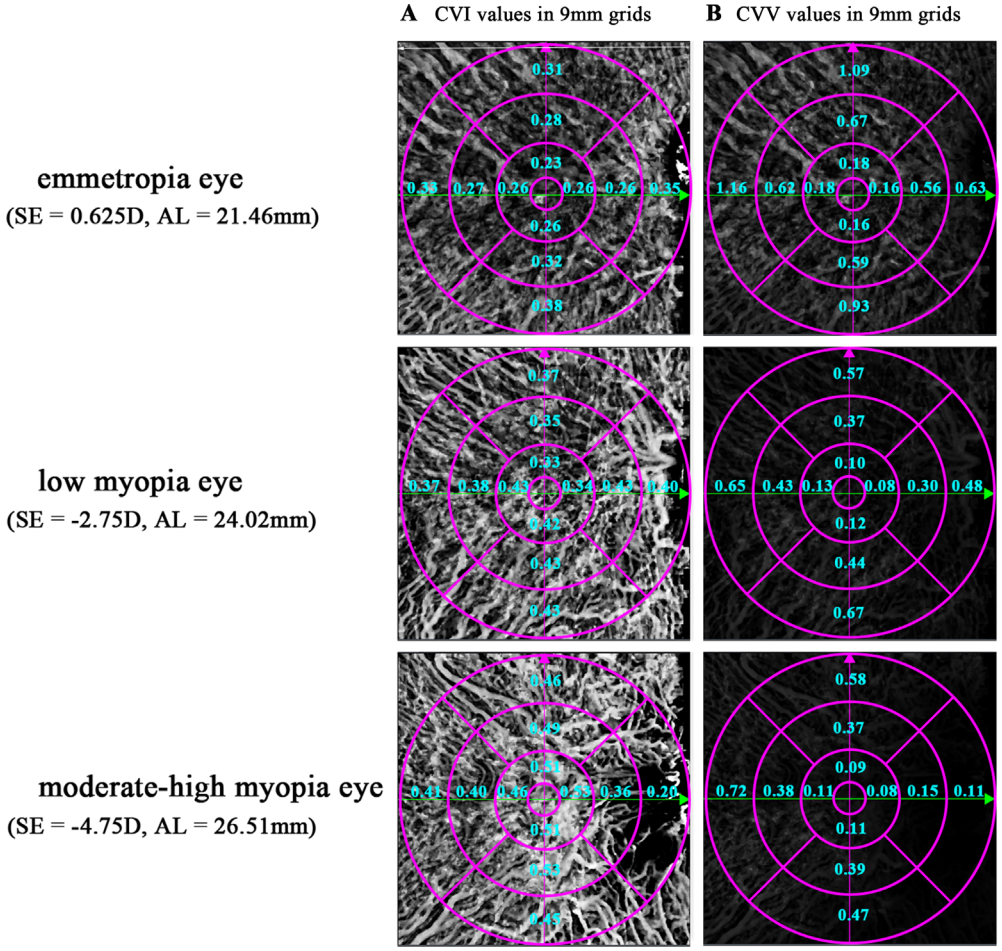

Figure 1. Example maps of the 3D-CVI. The *dark* and *light pixels* represent the choroidal parameter values of the corresponding location, such that the higher the value, the brighter the brightness. Shown are the 3D-CVI values (**A**) and CVV values (**B**) at the 9 × 9-mm ETDRS grid for three representative subjects.

the standard axial length of the system, the near-periphery region was excluded to ensure a more accurate quantitative analysis.

Statistical Analysis

R 3.5.1 (R Foundation for Statistical Computing, Vienna, Austria) and PASS 15.0 (NCSS Statistical Software, Kaysville, UT, USA) were used to perform statistical analyses. The Shapiro–Wilk test was used to assess the normality of the data distribution prior to statistical analysis. The generalized estimation equation (GEE) was used to compare differences among groups and to evaluate the association of the 3D-CVI (dependent factor) with biometric parameters (independent factors) in univariate analyses. Also, the paired *t*-test was used to assess the changing trend of choroidal parameters from the fovea to the perifovea. As appropriate, Bonferroni correction was conducted for multiplicity. Independent risk factors influencing the 3D-CVI were determined using stepwise multiple regression.

Finally, after adjusting sex, age and BMI, the parameters which were significantly correlated with the 3D-CVI in the univariate analysis (AL and SE) were further analyzed with restricted cubic splines analysis with four knots at the 5th, 35th, 65th, and 95th percentiles. Segmented regression was used to examine the threshold effects of AL and SE on the 3D-CVI according to the smooth curve fitting. The threshold level (turning point) of AL and SE at which the relationship among AL, SE, and the 3D-CVI began to change and became notable was determined by trial and error. Two-tailed $P < 0.05$ was considered statistically significant.[29,30]

Results

Of the 154 initial participants, we excluded nine due to poor cooperation and two due to poor OCT image quality. All images were accurately segmented by artificial intelligence, and no image was manually segmented by doctors. A total of 274 eyes (143 children; 78 boys and 65 girls) were finally enrolled with a mean age of 9.36 ± 2.10 years (detailed demographic information is presented in Supplementary Table S1). According to the SE of each eye, 56 eyes (0.10 ± 0.04 D), 151 eyes (−1.46 ± 0.06 D), and 67 eyes (−4.50 ± 1.15D) were assigned to the EM, LM, and MHM groups, respectively.

Age, body height, and weight were significantly lower in the LM and EM groups than in the MHM group (all $P < 0.05$), but no significant differences were found between the LM and EM groups (Supplementary Table S1), and the MHM group had significantly deeper anterior chamber depth

Table 1. Choroidal Parameters Among Participants With Different Refractive Errors

					LM Vs. EM			MHM Vs. EM			MHM Vs. LM			*P*, Group Parafovea and Perifovea Comparisons		
		EM	LM	MHM	β	95% CI	*P*	β	95% CI	*P*	β	95% CI	*P*	EM	LM	MHM
Parafoveal Quadrants																
Superior																
	CSV	0.19 ± 0.01	0.16 ± 0.01	0.14 ± 0.01	−0.04	−0.06 to −0.02	<0.001	−0.07	−0.09 to −0.04	<0.001	−0.02	−0.04 to 0.00	0.022			
	CVV	0.10 ± 0.00	0.09 ± 0.00	0.08 ± 0.00	−0.02	−0.03 to −0.01	<0.001	−0.02	−0.04 to −0.01	<0.001	−0.01	−0.02 to 0.00	0.070			
	CVI	0.36 ± 0.01	0.37 ± 0.01	0.38 ± 0.01	0.02	0.00 to 0.03	0.064	0.03	0.00 to 0.05	0.03	0.01	−0.01 to 0.03	0.622			
Temporal																
	CSV	0.21 ± 0.01	0.17 ± 0.01	0.15 ± 0.01	−0.05	−0.07 to −0.03	<0.001	−0.08	−0.11 to −0.06	<0.001	−0.03	−0.05 to −0.01	<0.001			
	CVV	0.11 ± 0.00	0.10 ± 0.00	0.09 ± 0.00	−0.01	−0.02 to −0.01	0.004	−0.03	−0.04 to −0.02	<0.001	−0.01	−0.02 to −0.01	<0.001			
	CVI	0.36 ± 0.01	0.37 ± 0.01	0.38 ± 0.01	0.02	0.00 to 0.03	0.060	0.03	0.01 to 0.05	0.014	0.01	−0.01 to 0.03	0.410			
Inferior																
	CSV	0.18 ± 0.01	0.15 ± 0.01	0.14 ± 0.01	−0.04	−0.05 to −0.02	<0.001	−0.07	−0.10 to −0.05	<0.001	−0.04	−0.06 to −0.02	<0.001			
	CVV	0.10 ± 0.00	0.09 ± 0.00	0.08 ± 0.00	−0.01	−0.02 to −0.01	<0.001	−0.03	−0.04 to −0.02	<0.001	−0.01	−0.03 to 0.00	0.018			
	CVI	0.37 ± 0.01	0.38 ± 0.01	0.38 ± 0.01	0.01	0.00 to 0.03	0.110	0.03	0.00 to 0.05	0.072	0.01	−0.01 to 0.03	0.546			
Nasal																
	CSV	0.16 ± 0.01	0.13 ± 0.01	0.11 ± 0.01	−0.04	−0.05 to −0.02	<0.001	−0.06	−0.08 to −0.04	<0.001	−0.03	−0.05 to 0.00	0.020			
	CVV	0.09 ± 0.00	0.08 ± 0.00	0.07 ± 0.00	−0.02	−0.03 to −0.01	<0.001	−0.03	−0.04 to −0.02	<0.001	−0.01	−0.02 to 0.00	0.050			
	CVI	0.39 ± 0.01	0.40 ± 0.01	0.40 ± 0.01	0.01	−0.01 to 0.03	0.868	0.02	−0.01 to 0.05	0.236	0.01	−0.01 to 0.03	0.390			
Perifoveal Quadrants																
Superior																
	CSV	0.19 ± 0.01	0.15 ± 0.01	0.14 ± 0.01	−0.13	−0.19 to −0.07	<0.001	−0.2	−0.26 to 0.13	<0.001	−0.07	−0.12 to −0.01	0.018	0.016	0.004	0.669
	CVV	0.10 ± 0.00	0.09 ± 0.00	0.09 ± 0.00	−0.04	−0.06 to −0.02	<0.001	−0.06	−0.08 to −0.03	<0.001	−0.02	−0.04 to 0.00	0.094	0.265	0.495	0.014
	CVI	0.36 ± 0.01	0.38 ± 0.01	0.39 ± 0.01	0.02	0.01 to 0.03	<0.001	0.03	0.02 to 0.05	<0.001	0.01	0.00 to 0.02	0.108	0.051	0.275	0.575
Temporal																
	CSV	0.21 ± 0.01	0.17 ± 0.01	0.16 ± 0.01	−0.14	−0.19 to −0.08	<0.001	−0.22	−0.30 to −0.14	<0.001	−0.09	−0.15 to −0.03	0.008	0.743	0.009	<0.001
	CVV	0.11 ± 0.00	0.10 ± 0.00	0.09 ± 0.00	−0.05	−0.07 to −0.03	<0.001	−0.08	−0.12 to −0.05	<0.001	−0.04	−0.07 to −0.01	0.026	0.043	0.167	0.446
	CVI	0.35 ± 0.01	0.36 ± 0.01	0.36 ± 0.01	0.01	0.00 to 0.02	0.018	0.02	0.00 to 0.04	0.056	0.01	−0.01 to 0.02	0.782	0.871	0.116	<0.001
Inferior																
	CSV	0.17 ± 0.01	0.14 ± 0.01	0.13 ± 0.01	−0.11	−0.16 to −0.07	<0.001	−0.21	−0.28 to −0.15	<0.001	−0.10	−0.16 to −0.04	<0.001	<0.001	<0.001	0.048
	CVV	0.10 ± 0.00	0.09 ± 0.00	0.08 ± 0.00	−0.04	−0.06 to −0.02	<0.001	−0.08	−0.11 to −0.05	<0.001	−0.04	−0.07 to −0.01	0.020	0.07	0.025	0.492
	CVI	0.38 ± 0.01	0.39 ± 0.01	0.40 ± 0.01	0.01	0.00 to 0.03	0.062	0.03	0.01 to 0.04	<0.001	0.01	0.00 to 0.03	0.096	<0.001	<0.001	<0.001
Nasal																
	CSV	0.11 ± 0.01	0.10 ± 0.00	0.09 ± 0.01	−0.06	−0.11 to −0.02	0.020	−0.13	−0.19 to −0.06	<0.001	−0.06	−0.12 to −0.01	0.028	<0.001	<0.001	<0.001
	CVV	0.08 ± 0.00	0.07 ± 0.00	0.06 ± 0.00	−0.05	−0.08 to −0.03	<0.001	−0.09	−0.13 to −0.05	<0.001	−0.04	−0.08 to 0.00	0.062	<0.001	<0.001	<0.001
	CVI	0.44 ± 0.01	0.43 ± 0.01	0.42 ± 0.01	−0.00	−0.02 to 0.01	>0.99	−0.00	−0.03 to 0.02	>0.99	0.00	−0.02 to 0.02	>0.99	<0.001	<0.001	<0.001

CI, confidence interval.

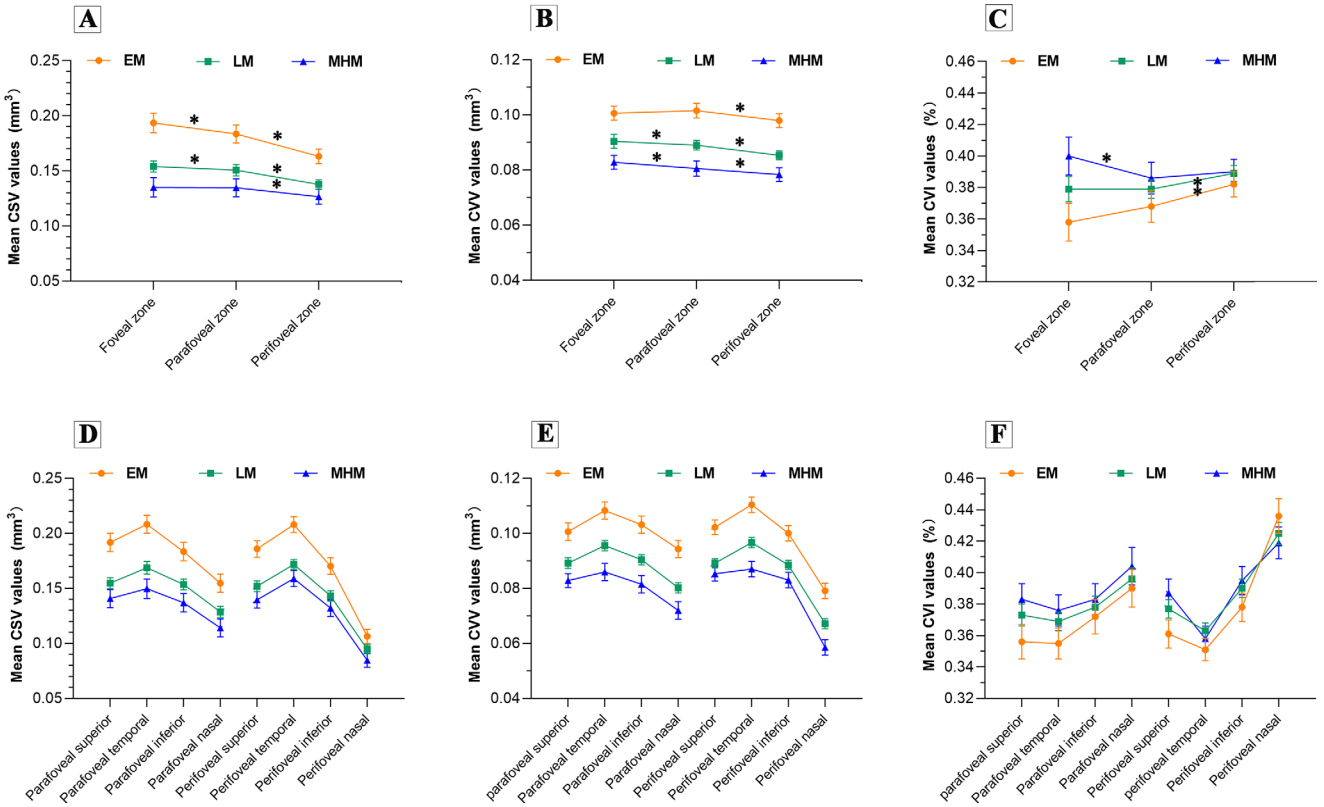

Figure 2. Mean CSV (**A**, **D**), CVV (**B**, **E**), and 3D-CVI (**C**, **F**) values across different eccentricities (**A–C**) and quadrants (**D–F**) among three different refractive groups. *Error bars* indicate the standard error of the mean. *$P < 0.05$.

compared to the LM group ($P < 0.05$). There were no significant differences in Km, CCT, WTW, lens thickness, gender, and BMI values among the three groups (all $P > 0.05$) (Supplementary Table S2).

Table 1 compares choroidal parameters in the eccentricities and quadrants among participants with different refractive errors. GEE analysis revealed that all of the CVV and CSV parameters were significantly lower in the LM and MHM groups than in the EM group. In contrast, most of the 3D-CVI parameters were significantly higher in the LM and MHM groups than in the EM group (all $P < 0.05$, after multiplicity correction). Compared to the LM group, the MHM group had a significantly lower CSV in all regions and lower CVV in most regions (except for the fovea circle region and the superior and nasal quadrants of the parafovea and perifovea; all $P < 0.05$, after multiplicity correction). Notably, the degree of decline in CSV was greater than the decline in CVV in all groups ($\beta_{CSV} < \beta_{CVV}$), indicating that the decrease in the choroidal stroma was greater than the decrease in choroidal vessels.

The 3D-CVIs of the EM and LM groups gradually increased from the fovea to the perifovea, and only the 3D-CVIs of the perifovea were significantly higher than the parafovea ($P < 0.05$). The 3D-CVIs of the MHM group first decreased and then increased (Figs. 2A–C), and the 3D-CVIs of the parafovea were significantly lower than for the fovea ($P < 0.05$) (Supplementary Table S3). The nasal quadrant had the greatest 3D-CVIs and lowest CSVs and CVVs, whereas the temporal quadrant had the lowest 3D-CVIs and greatest CSVs and CVVs in all group (Figs. 2D–F). For the CVI and CSV, the eccentricity change was largely contributed to by the nasal and inferior quadrants; for the CVV, the eccentricity change was largely contributed to by the nasal quadrant.

Table 2. Associations Between the Ocular Parameters and 3D-CVIs of Three Eccentricity Zones

Factors	β Coefficient	95% CI	*P*
Foveal zone			
AL	0.021	0.011 to 0.030	<0.001
SE	−0.011	−0.018 to −0.005	<0.001
Parafoveal zone			
AL	0.016	0.009 to 0.022	<0.001
SE	−0.007	−0.011 to −0.002	0.003
Perifoveal zone			
AL	0.010	0.003 to 0.016	0.003
SE	−0.006	−0.091 to −0.002	<0.001

Univariable analysis revealed that the 3D-CVIs of the three eccentricity zones positively correlated with AL and negatively correlated with SE (all $P < 0.05$) (Table 2). Stepwise multiple linear regression analysis indicated that AL was an independent factor associated with the 3D-CVIs of foveal ($\beta = 0.022$) and parafoveal ($\beta = 0.013$) zones (all $P < 0.05$), but not the perifoveal zone (Table 3). With the elongation of AL, the 3D-CVI values of the foveal and parafoveal zones increased. Restricted cubic spline analysis further revealed that only the SE and 3D-CVI exhibited nonlinear relationships. The 3D-CVI increased with increasing SE when SE was less than the turning point and decreased when the SE was greater than the turning point (turning

Table 3. Stepwise Multiple Linear Regression Analysis of Independent Factors Affecting the 3D-CVIs in Three Eccentricity Zones

Factors	β Coefficient	Standard Error	95% CI	*P*
Foveal zone				
Intercept	0.006	0.188	−0.363 to 0.375	0.974
AL	0.022	0.008	0.007 to 0.037	0.005
Parafoveal zone				
Intercept	0.058	0.148	−0.231 to 0.348	0.693
AL	0.013	0.006	0.001 to 0.025	0.029

points were −5.25D, −5.125D, and −2.00D for the foveal, parafoveal, and perifoveal regions, respectively) (Fig. 3). The threshold effect of SE on the 3D-CVI of each concentric annular zone was significant (all $P < 0.05$).

Discussion

In this study, myopic eyes exhibited reduced choroidal vessel and stroma volume and an increased 3D-CVI. Further, restricted cubic spline analysis indicated that the SEs and 3D-CVIs of all eccentricity zones (fovea, parafovea, and perifovea) exhibited nonlinear relationships. To the best of our knowledge, this study is the first to investigate the topographic alterations of choroidal vessel parameters in children with different degrees of myopia, and we found the nonlinear relationship between SE and the 3D-CVI. These fundings provide novel insight into further understanding the potential pathophysiology of myopia, which can help in the identification of biomarkers for clinical management and disease prognostication.

The higher the degree of myopia, the greater the age, weight, and height, which was consistent with the results reported in the previous literature.[26–28] Also, our results indicate that both CVV and CSV were decreased in myopic eyes, which was in line with previous reports.[19,20,29] We found that, in most regions, the 3D-CVI of the more severe myope was greater than that of the less severe myope ($3D\text{-}CVI_{MHM} > 3D\text{-}CVI_{LM} > 3D\text{-}CVI_{EM}$). In addition, the group with more severe myopia exhibited a greater diminution of CSV relative to CVV, which explains the higher 3D-CVIs. These results are consistent with previous reports on myopic eyes.[29–31] Liu et al.[19] reported a lower 3D-CVI and greater reduction in CVV than CSV of eyes with high myopia compared to eyes with low-to-moderate myopia. The patients predominantly were moderate-to-high myopia in that study (mean SE of −5.95 D), whereas those in the current study were low myopia (mean SE of −1.90 D). The difference between the two studies may be due to the different degrees of myopia (SEs), which is supported by the nonlinear relationship results. Moreover, age is well established as a pivotal factor affecting the choroidal structure.[32] In previous reports that differed from the results of the present study,[15,20] the mean ages of subjects in the studies by Wu et al.[15] and Xu et al.[20] were 13.1 ± 1.9 years and 29.43 ± 10.18 years, respectively, which was older than that of our current study (mean age of 9.36 ± 2.10 years). Li et al.[33] reported that the 3D-CVI increased with age, and there was a greater decrease in the stromal area than in the luminal area, resulting an increase in the 3D-CVI. The structural differences in choroid between children and adults may also be a reason for the difference in 3D-CVI results and warrants further investigation.

In addition, we also found that CSV, CVV, and the 3D-CVI have regional variations in different eccentricities and quadrants. Regarding quadrantal variation, the greatest CVVs and CSVs were in the temporal quadrant, and the lowest CVVs and CSVs were in the nasal quadrant. The quadrant-related variation trend was consistent with a previous study that described choroidal thickness characteristics across different quadrants in Chinese children.[34,35] The optic nerve is located on the nasal side, and the choroid gradually thins toward the optic disc until it disappears,[36,37] which may partly explain the abovementioned results. The lowest and highest 3D-CVIs were observed in the temporal and nasal quadrants, respectively, and the quadrantal variation was similar to that reported by Yazdani et al.[29] and Singh et al.[17] This phenomenon may be underpinned by the greater number of non-vascular smooth muscle cells in the temporal quadrant than in the nasal quadrant.[38]

Concerning alterations in eccentricities, the CSVs and CVVs of all groups gradually decreased from the fovea to the perifovea, consistent with previous reports.[31,43] Alsharreef et al.[39] evaluated choroidal morphologic features using OCT and reported a progressive reduction of the choroidal medium and large vessel thickness from the fovea to perifovea. Yazdani et al.[29] obtained similar results on luminal and stromal thickness using the binarization method. In addition, we also found a gradual increase in the 3D-CVIs from fovea to perifovea in the EM and LM groups, consistent with previous studies in healthy participants.[29,32] The variation trend discrepancy among CSV, CVV, and the 3D-CVI may be due to the fact that the foveal zone has more stromal components than the perifoveal zone.[38,40] Of note, the 3D-CVIs of the MHM group first decreased and then increased from fovea

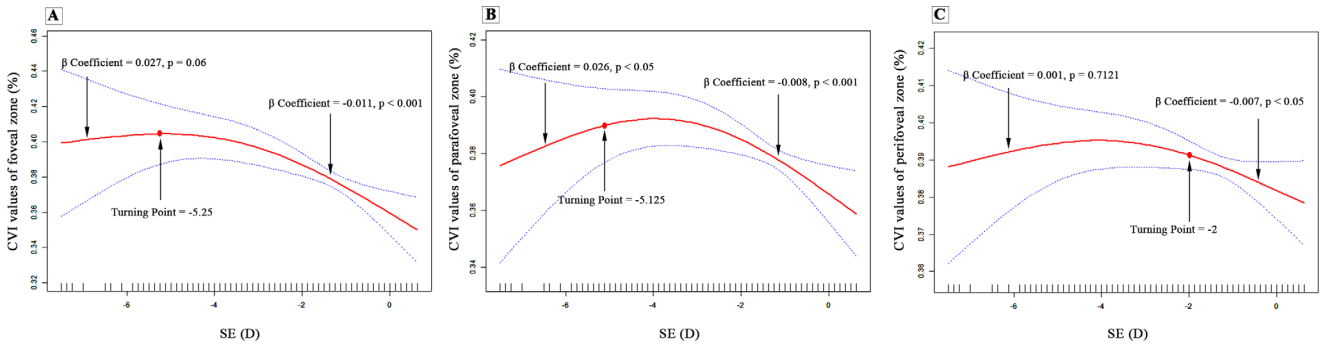

Figure 3. Relationship between SE and 3D-CVI values of the foveal (**A**), parafoveal (**B**), and perifoveal zones (**C**) in a restricted cubic spline plot. The *red line* represents the estimate, and the *blue dotted line* represents the upper and lower limits of the 95% confidence intervals.

to perifovea. In contrast to the consistent 3D-CVI quadrant-related variation trend among the three groups, the different 3D-CVI eccentricity-related variation trend among the MHM group compared to the EM and LM group suggested that variation of the 3D-CVIs in different eccentricities may be more sensitive than that in quadrants.

Correlation analysis revealed that AL and SE were significantly associated with the 3D-CVI in the foveal, parafoveal, and perifoveal zones. Stepwise multiple linear regression analysis revealed that prolonged AL was the main factor influencing the 3D-CVI of the foveal and parafoveal zones. These results are similar to those of previous reports on myopic eyes. Yazdani et al.[29] and Alshareef et al.[31] reported that a longer AL was associated with greater choroidal vascularity in myopes. At the same time, a negative correlation was observed between AL and the 3D-CVI.[41] Breher et al.[42] reported that the 3D-CVI exhibited a bidirectional correlation with AL; that is, AL was positively correlated with the foveal 3D-CVI and negatively correlated with the peripheral 3D-CVI.[42] In this study, we used volumetric data to assess the choroidal structure, which may be more informative than the local areal metric. These reasons may partly explain the disparities in the results among different studies.

Because most of the previous association studies followed the hypothesis of linear trend,[15,33,43] some potential information (such as nonlinear relationships) may be missed. Hence, to determine how the 3D-CVI varied, we used restricted cubic spline analysis to further characterize the association between the 3D-CVI and the ocular parameters (AL and SE) that showed a significant association in the univariate analysis. The analysis indicated that the 3D-CVI increased with increasing SE when SE was less than the turning point and decreased when SE was greater than the turning point (turning points were −5.25 D, −5.125 D, and −2.00 D for the foveal, parafoveal, and perifoveal regions, respectively). To the best of our knowledge, the "quadratic" correlation between SE and the 3D-CVI has not been reported to date. We speculated that the CSV decreased more than the CVV in the early stages of myopia, leading to an increase in the 3D-CVI. When the severity of myopia exceeded a certain threshold, a greater reduction in CVV than CSV resulted in a decreased 3D-CVI. These results provide novel insight into the pathophysiology and pathogenesis of myopia and may contribute to a deeper understanding of the choroidal internal structural changes related to myopia.

Many studies have reported that the choroid plays a pivotal role in myopia onset and development. The choroid is divided into three layers from the inside out: capillary layer, Sattler's large vessel layer, and Haller's medium-to-small vascular layer. Changes in the choroidal thickness associated with myopia have been reported to result predominantly from Sattler's and Haller's layers.[44] Therefore, we used volumetric scans to reflect the changes in Sattler's and Haller's layers. This novel method demonstrated better repeatability and less variability than conventional local scans,[19] thus providing more accurate and comprehensive information about the relative changes in choroidal vessels and stroma and being helpful in revealing the potential role of choroidal changes in myopes.

Given that the choroidal vessels are the primary source of nutrients and oxygen to the surrounding retina and sclera, knowledge of the changes in the choroidal vasculature and their interaction with myopia may reveal potential pathophysiological mechanisms and help to prevent and treat myopia. Although the exact mechanism that causes the choroidal vascular changes associated with myopia in children remains unclear, our results suggest that the choroidal vessels may supply adequate nutrients and oxygen to the surrounding tissues at the onset of myopia. Some scholars have found that children with low myopia have relatively normal visual function compared with children with high myopia, which further supports the above conjecture.[45] As the disease progresses, the CVV gradually reduces and may become decompensated, failing to provide adequate nutrition and leading to scleral thinning and worsening of myopia.

Limitations

This study has several limitations. First, due to its cross-sectional design, cause-and-effect relationships cannot be identified. Further longitudinal studies are warranted to elucidate the association between the choroidal structure and myopia progression. Second, as signal attenuation occurs with depth penetration, quantifying the blood flow of complex choroidal capillaries is inaccurate; therefore, we excluded it from our study. Third, because high myopia is less common in primary school students,[46] our study lacked a sufficient sample size of children with high myopia (nine cases), which may account for the wide 95% confidence interval. Therefore, future studies are required to examine the variations in these choroid parameters in larger populations, such as those with high myopia and hyperopia. Finally, the population of this study was limited to a single ethnicity, so further studies should enroll multiethnic populations.

Conclusions

Our study revealed a significantly lower CVV and CSV and higher 3D-CVI in myopic children. In addition, with myopia development, 3D-CVI eccentricity variation characteristics also changed (first decreased and then increased from the fovea to the perifovea). Future longitudinal follow-up studies are warranted to gain further insight into the association between choroidal structure and myopia.

Acknowledgments

The authors thank all the patients for their participation and the research staff from the Eye, Ear, Nose, and Throat Hospital of Fudan University for their contribution to this study.

Supported by grants from the National Natural Science Foundation of China (81770955), Joint Research Project of New Frontier Technology in Municipal Hospitals (SHDC12018103), Shanghai Rising-Star Program (21QA1401500), Shanghai Natural Science Foundation (23ZR1409200), Project of Shanghai Science and Technology (20410710100), Clinical Research Plan of SHDC (SHDC2020CR1043B), Project of Shanghai Xuhui District Science and Technology (2020-015), and Shanghai Municipal Commission of Health and Family Planning (202040285).

Disclosure: **F. Liu**, None; **Y. Ye**, None; **W. Yang**, None; **J. Wang**, None; **Y. Xu**, None; **Y. Zhao**, None; **M. Li**, None; **Z. Chen,** None; **Y. Shen**, None; **M. Li**, None; **X. Zhou**, None

References

1. Holden BA, Fricke TR, Wilson DA, et al. Global prevalence of myopia and high myopia and temporal trends from 2000 through 2050. *Ophthalmology*. 2016;123(5):1036–1042.

2. Flitcroft DI. The complex interactions of retinal, optical and environmental factors in myopia aetiology. *Prog Retin Eye Res*. 2012;31(6):622–660.
3. Ruiz-Medrano J, Montero JA, Flores-Moreno I, Arias L, Garcia-Layana A, Ruiz-Moreno JM. Myopic maculopathy: current status and proposal for a new classification and grading system (ATN). *Prog Retin Eye Res*. 2019;69:80–115.
4. Zhang Y, Wildsoet CF. RPE and choroid mechanisms underlying ocular growth and myopia. *Prog Mol Biol Transl Sci*. 2015;134:221–240.
5. Morgan IG, Ohno-Matsui K, Saw SM. Myopia. *Lancet*. 2012;379(9827):1739–1748.
6. Nickla DL, Wallman J. The multifunctional choroid. *Prog Retin Eye Res*. 2010;29(2):144–168.
7. Chiang ST, Phillips JR, Backhouse S. Effect of retinal image defocus on the thickness of the human choroid. *Ophthalmic Physiol Opt*. 2015;35(4):405–413.
8. Read SA, Collins MJ, Sander BP. Human optical axial length and defocus. *Invest Ophthalmol Vis Sci*. 2010;51(12):6262–6269.
9. Wu H, Chen W, Zhao F, et al. Scleral hypoxia is a target for myopia control. *Proc Natl Acad Sci USA*. 2018;115(30):E7091–E7100.
10. Summers JA. The choroid as a sclera growth regulator. *Exp Eye Res*. 2013;114:120–127.
11. Agrawal R, Gupta P, Tan KA, Cheung CMG, Wong T-Y, Cheng C-Y. Choroidal vascularity index as a measure of vascular status of the choroid: measurements in healthy eyes from a population-based study. *Sci Rep*. 2016;6:21090.
12. Betzler BK, Ding J, Wei X, et al. Choroidal vascularity index: a step towards software as a medical device. *Br J Ophthalmol*. 2022;106(2):149–155.
13. Koh L, Agrawal R, Khandelwal N, Sai CL, Chhablani J. Choroidal vascular changes in age-related macular degeneration. *Acta Ophthalmol*. 2017;95(7):e597–e601.
14. Tan KA, Laude A, Yip V, et al. Choroidal vascularity index - a novel optical coherence tomography parameter for disease monitoring in diabetes mellitus? *Acta Ophthalmol*. 2016;94(7):e612–e616.
15. Wu H, Xie Z, Wang P, et al. Differences in retinal and choroidal vasculature and perfusion related to axial length in pediatric anisomyopes. *Invest Ophthalmol Vis Sci*. 2021;62(9):40.
16. Ouyang Y, Heussen FM, Mokwa N, et al. Spatial distribution of posterior pole choroidal thickness by spectral domain optical coherence tomography. *Invest Ophthalmol Vis Sci*. 2011;52(9):7019–7026.
17. Singh SR, Invernizzi A, Rasheed MA, et al. Wide-field choroidal vascularity in healthy eyes. *Am J Ophthalmol*. 2018;193:100–105.
18. Nivison-Smith L, Khandelwal N, Tong J, Mahajan S, Kalloniatis M, Agrawal R. Normal aging changes in the choroidal angioarchitecture of the macula. *Sci Rep*. 2020;10(1):10810.
19. Liu L, Zhu C, Yuan Y, et al. Three-dimensional choroidal vascularity index in high myopia using swept-source optical coherence tomography. *Curr Eye Res*. 2022;47(3):484–492.
20. Xu A, Sun G, Duan C, Chen Z, Chen C. Quantitative assessment of three-dimensional choroidal vascularity and choriocapillaris flow signal voids in myopic patients using SS-OCTA. *Diagnostics (Basel)*. 2021;11(11):1948.
21. Lee SW, Yu SY, Seo KH, Kim ES, Kwak HW. Diurnal variation in choroidal thickness in relation to sex, axial length, and baseline choroidal thickness in healthy Korean subjects. *Retina*. 2014;34(2):385–393.
22. Read SA, Pieterse EC, Alonso-Caneiro D, et al. Daily morning light therapy is associated with an increase in choroidal thickness in healthy young adults. *Sci Rep*. 2018;8(1):8200.
23. Lan W, Feldkaemper M, Schaeffel F. Bright light induces choroidal thickening in chickens. *Optom Vis Sci*. 2013;90(11):1199–1206.
24. Atchison DA. Optical models for human myopic eyes. *Vision Res*. 2006;46(14):2236–2250.
25. Agrawal R, Ding J, Sen P, et al. Exploring choroidal angioarchitecture in health and disease using choroidal vascularity index. *Prog Retin Eye Res*. 2020;77:100829.
26. Bruce A, Mojarrad NG, Santorelli G. Association of anthropometric measures across the life-course with refractive error and ocular biometry at age 15 years. *BMC Ophthalmol*. 2020;20(1):269.
27. Nakao SY, Miyake M, Hosoda Y, et al. Myopia prevalence and ocular biometry features in a general Japanese population: the Nagahama Study. *Ophthalmology*. 2021;128(4):522–531.
28. Tideman J, Polling JR, Vingerling JR, et al. Axial length growth and the risk of developing myopia in European children. *Acta Ophthalmol*. 2018;96(3):301–309.
29. Yazdani N, Ehsaei A, Hoseini-Yazdi H, Shoeibi N, Alonso-Caneiro D, Collins MJ. Wide-field choroidal thickness and vascularity index in myopes and emmetropes. *Ophthalmic Physiol Opt*. 2021;41(6):1308–1319.
30. Gupta P, Thakku SG, Saw SM, et al. Characterization of choroidal morphologic and vascular features in young men with high myopia using spectral-domain optical coherence tomography. *Am J Ophthalmol*. 2017;177:27–33.
31. Alshareef RA, Khuthaila MK, Goud A, Vupparaboina KK, Jana S, Chhablani J. Subfoveal choroidal vascularity in myopia: evidence from spectral-domain optical coherence tomography. *Ophthalmic Surg Lasers Imaging Retina*. 2017;48(3):202–207.
32. Goud A, Singh SR, Sahoo NK, et al. New insights on choroidal vascularity: a comprehensive topographic approach. *Invest Ophthalmol Vis Sci*. 2019;60(10):3563–3569.
33. Li Z, Long W, Hu Y, Zhao W, Zhang W, Yang X. Features of the choroidal structures in myopic children based on image binarization of optical coherence tomography. *Invest Ophthalmol Vis Sci*. 2020;61(4):18.
34. Zhang JM, Wu JF, Chen JH, et al. Macular choroidal thickness in children: the Shandong Children Eye Study. *Invest Ophthalmol Vis Sci*. 2015;56(13):7646–7652.
35. He X, Jin P, Zou H, et al. Choroidal thickness in healthy Chinese children aged 6 to 12: the Shanghai Children Eye Study. *Retina*. 2017;37(2):368–375.
36. Kubota T, Jonas JB, Naumann GO. Decreased choroidal thickness in eyes with secondary angle closure glaucoma. An aetiological factor for deep retinal changes in glaucoma? *Br J Ophthalmol*. 1993;77(7):430–432.
37. Yamashita T, Sakamoto T, Yoshihara N, et al. Correlations between local peripapillary choroidal thickness and axial length, optic disc tilt, and papillo-macular position in young healthy eyes. *PLoS One*. 2017;12(10):e0186453.
38. May CA. Non-vascular smooth muscle cells in the human choroid: distribution, development and further characterization. *J Anat*. 2005;207(4):381–390.
39. Alshareef RA, Khuthaila MK, Januwada M, Goud A, Ferrara D, Chhablani J. Choroidal vascular analysis in myopic eyes: evidence of foveal medium vessel layer thinning. *Int J Retina Vitreous*. 2017;3:28.
40. Yiu G, Vuong VS, Oltjen S, et al. Effect of uveal melanocytes on choroidal morphology in rhesus macaques and humans on enhanced-depth imaging optical coherence tomography. *Invest Ophthalmol Vis Sci*. 2016;57(13):5764–5771.
41. Wu H, Zhang G, Shen M, et al. Assessment of choroidal vascularity and choriocapillaris blood perfusion in anisomy-

Investigative Ophthalmology & Visual Science

opic adults by SS-OCT/OCTA. *Invest Ophthalmol Vis Sci*. 2021;62(1):8.

42. Breher K, Terry L, Bower T, Wahl S. Choroidal biomarkers: a repeatability and topographical comparison of choroidal thickness and choroidal vascularity index in healthy eyes. *Transl Vis Sci Technol*. 2020;9(11):8.
43. Liu F, Niu L, Guo J, et al. Quantitative evaluation of retinal and choroidal vascularity and retrobulbar blood flow in patients with myopic anisometropia by CDI and OCTA. *Br J Ophthalmol*. 2023;107(8):1172–1177.
44. Zhao J, Wang YX, Zhang Q, et al. Macular choroidal small-vessel layer, Sattler's layer and Haller's layer thicknesses: the Beijing Eye Study. *Sci Rep*. 2018;8(1):4411.
45. Flitcroft DI, Adams GG, Robson AG, Holder GE. Retinal dysfunction and refractive errors: an electrophysiological study of children. *Br J Ophthalmol*. 2005;89(4):484–488.
46. Wang SK, Guo Y, Liao C, et al. Incidence of and factors associated with myopia and high myopia in Chinese children, based on refraction without cycloplegia. *JAMA Ophthalmol*. 2018;136(9):1017–1024.

Investigative Ophthalmology & Visual Science